

# Optical Communications with Relative Intensity Noise: Channel Modeling and Information Rates

Felipe Villenas, Yunus Can Gültekin, and Alex Alvarado

Department of Electrical Engineering, Eindhoven University of Technology, the Netherlands

{f.i.villenas.cortez, y.c.g.gultekin, a.alvarado}@tue.nl

**Abstract**—We consider optical communications with intensity modulation and direct detection affected by laser relative intensity noise (RIN). Starting from a continuous-time waveform model, we derive an equivalent discrete-time channel model. As a result of RIN, the resulting channel model exhibits signal-dependent noise with memory. Unlike the commonly-assumed model in the literature, the conditional variance of this noise term has a polynomial dependence on the symbol of interest. Finally, we study achievable information rates for this channel under practically-relevant system parameters. We take a mismatched decoding approach and compute the generalized mutual information (GMI) using a memoryless decoding metric. Our numerical results show that when the memory in the channel is ignored by the receiver, GMI saturates as the constellation size increases, and thus, dense constellations do not offer gains. We also show that this saturation results from nonsymmetric nonvanishing contributions of the symbols to the GMI.

**Index Terms**—Optical communications, intensity modulation and direct detection, relative intensity noise, achievable information rates, mismatched decoding, generalized mutual information.

## I. INTRODUCTION

FUELED by the exploding demand from artificial intelligence applications, the need for increasing data rates in short-reach data center interconnects (DCI) is unstoppable [1]. Maintaining relatively low hardware costs is also of key importance, and thus, the vast majority of these optical links employ intensity-modulation (IM) and direct-detection (DD) where only the amplitude of the transmitted optical light is modulated to carry information [2]. Pulse amplitude modulation (PAM) is typically employed in these systems, enabling low-complexity transceivers with low power consumption [3].

Rates up to 200 Gbps have been shown to be feasible for IM-DD systems with PAM-4 [4]. To achieve 400 Gbps, doubling the symbol rate is the most straightforward option. However, increasing the symbol rate also means integrating the noise power spectral density (PSD) over a larger bandwidth. Thus, the transmit power must also increase to maintain or improve the signal-to-noise ratio. This increase in signal power leads to the generation of signal-dependent noise caused by relative intensity noise (RIN) of the laser.

RIN is typically measured from a constant light source (e.g., a laser), without an information-carrying signal [5], [6]. RIN

is then modeled as memoryless with power proportional to the square of the instantaneous light intensity [5]. In PAM systems, this assumption on RIN results in a model widely used in the literature (see, e.g., [7]–[9]), where the noise power is proportional to the square of the transmitted symbol. In this paper, we present a detailed analysis of RIN-dominated high-speed IM-DD systems. Starting from the continuous-time transfer characteristics of the signal processing blocks in the transceiver chain, we develop a discrete-time equivalent channel model that explicitly accounts for the statistics of the transmitted symbol sequence. The resulting model demonstrates that the commonly used signal-dependent noise model in the literature is imprecise, as it computes the noise statistics neglecting the properties of the information-carrying signal.

The contributions of this paper are threefold. Firstly, we develop a novel analytical discrete-time channel model for such systems. The proposed model—unlike the one often used in the literature [7]–[9]—is a channel with memory. Secondly, we show through numerical simulations that the proposed model accurately characterizes the signal-dependent noise for arbitrary continuous time PAM waveforms generated with band-limited pulses. Lastly, we evaluate achievable information rates (AIRs) of the proposed channel model using a mismatched decoding perspective, where the decoding metric is assumed to be memoryless. Our AIR results show that for typical practical system parameters, using  $M$ -PAM modulation formats with more than 8 points results in negligible gains.

The paper is organized as follows. The system model is described in Sec. II. The novel discrete-time channel model with memory is derived in Sec. III. The statistical properties of the noise and memory are investigated in Sec. IV. AIRs are studied in Sec. V before the conclusions are drawn in Sec. VI.

## II. SYSTEM MODEL

We consider the baseband equivalent IM-DD system shown in Fig. 1. We define the optical PAM- $M$  constellation by the random variable (RV)  $A \in \mathcal{A} = \{a_0, a_1, \dots, a_{M-1}\}$ , with  $a_n > 0$  for all  $n = 0, 1, \dots, M-1$  and  $|\mathcal{A}| = M$ . The outermost symbols of the optical constellation  $\mathcal{A}$  are determined by the optical modulation amplitude (OMA) and extinction ratio (ER), defined as

$$\text{OMA} \triangleq \max\{\mathcal{A}\} - \min\{\mathcal{A}\}, \text{ER} \triangleq \max\{\mathcal{A}\}/\min\{\mathcal{A}\}. \quad (1)$$

A sequence of optical PAM symbols  $\{A_m\}_{m \in \mathbb{Z}}$  is transmitted, where the elements  $A_m$  are independent and uniformly

arXiv:2603.08411v1 [cs.IT] 9 Mar 2026

This research is part of the project COMplexity-CONstrained LIght-coherent optical links (COCOLI) funded by Holland High Tech | TKI HSTM via the PPS allowance scheme for public-private partnerships, and of the project AISUSAT with grant ID OAARE97526 of the research programme AiNed XS Europe financed by the Dutch Research Council (NWO).

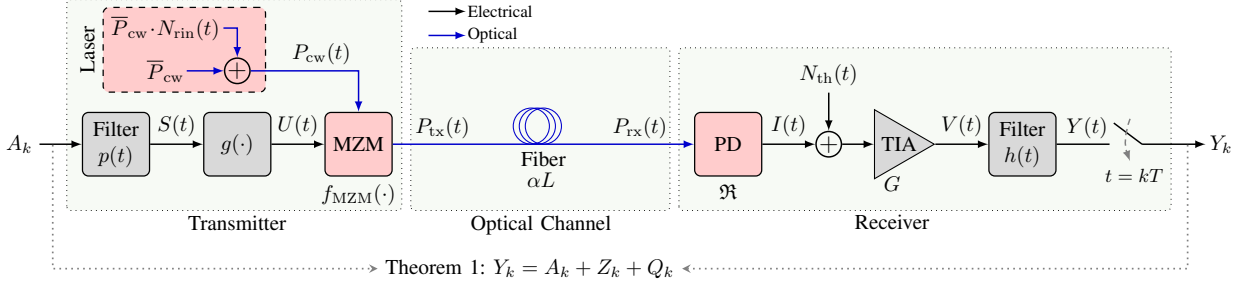


Fig. 1. Equivalent high-speed IM-DD system with laser RIN and external modulation.

distributed (i.u.d.) RVs. Pulse shaping with a filter impulse response  $p(t)$  is used. At the output of the transmitter filter, the generated waveform is

$$S(t) = \sum_{m \in \mathbb{Z}} A_m p(t - mT), \quad (2)$$

where  $T$  is the symbol period defined by the signaling rate  $R_s = 1/T$ . The filter  $p(t)$  is an arbitrary pulse shape that, in combination with the filter  $h(t)$  at the receiver (see Fig. 1) with  $\|h\|_2^2 = \int_{\mathbb{R}} h^2(t) dt = R_s$ , forms a combination that satisfies the zero intersymbol interference (ISI) Nyquist criterion, e.g., both can be root-raised-cosine (RRC) filters.

We consider a laser in continuous-wave (CW) operation alongside a Mach-Zehnder modulator (MZM) to modulate the amplitude of the optical wave. The output optical power of the laser can be modeled as

$$P_{\text{cw}}(t) = \bar{P}_{\text{cw}} (1 + N_{\text{rin}}(t)), \quad (3)$$

where  $N_{\text{rin}}(t)$  models the RIN. In this work, we model RIN as a continuous-time zero-mean white Gaussian random process [10, Ch. 3.3.6]. That is  $\mathbb{E}[N_{\text{rin}}(t)] = 0$ ,  $R_{\text{rin}}(\tau) = \frac{1}{2} N_0^{\text{rin}} \delta(\tau)$ , and  $S_{\text{rin}}(f) = \frac{1}{2} N_0^{\text{rin}}$ , where  $R_{\text{rin}}(\tau)$  and  $S_{\text{rin}}(f)$  are the autocorrelation function and double-sided PSD of  $N_{\text{rin}}(t)$ , resp. Thus,  $\bar{P}_{\text{cw}}$  in (3) is the laser's average optical power.

At the fiber input, the transmit signal  $P_{\text{tx}}(t)$  should be as close as possible to the PAM waveform  $S(t)$ . The device used for the electrical-to-optical conversion is an MZM in push-pull configuration, which has the optical power transfer function

$$f_{\text{MZM}}(U(t)) = \frac{P_{\text{tx}}(t)}{P_{\text{cw}}(t)} = \cos^2\left(\frac{\pi}{2V_\pi} U(t)\right), \quad (4)$$

where  $V_\pi$  is a modulator design parameter and  $U(t)$  is the electrical signal driving the relationship between the output  $P_{\text{tx}}(t)$  and the input  $P_{\text{cw}}(t)$ .

To mitigate the nonlinearities of the transfer function (4), a pre-distortion function  $g(\cdot)$  is applied to  $S(t)$  prior to modulation such that the MZM output is  $f_{\text{MZM}}(g(S(t))) \propto S(t)$ . Here, it is assumed that  $\text{ER} < \infty^1$  and that  $\min_{t \in \mathbb{R}} \{S(t)\} \geq 0$ . The constraint on the minimum value of  $S(t)$  is required to avoid distortion of the signal  $S(t)$  due to the positivity constraint of the optical power  $P_{\text{tx}}(t)$ .

<sup>1</sup>The case when  $\text{ER} \rightarrow \infty$  happens when  $\min\{A\} = 0$  and may only hold when using rectangular pulses with infinite bandwidth.

For the MZM transfer function (4), the optimum pre-distortion function  $g(\cdot)$ , for which  $f_{\text{MZM}}(g(S(t))) = S(t)$ , is

$$U(t) = g(S(t)) = -\frac{2V_\pi}{\pi} \arccos\left(\sqrt{\frac{S(t)}{\bar{P}_{\text{cw}}}}\right). \quad (5)$$

Using (4), the laser power in (3) will then be scaled as

$$P_{\text{tx}}(t) = P_{\text{cw}}(t) f_{\text{MZM}}(U(t)) = S(t) (1 + N_{\text{rin}}(t)). \quad (6)$$

The main application of high-speed IM-DD systems is intra-DCI for very limited reach, where the fiber length is expected to be  $L < 1$  km for 400 Gbps and beyond. We assume that the laser is operated in the O-band with wavelength 1310 nm, where chromatic dispersion is negligible [3, Sec. 3.3]. Thus, we only consider attenuation during fiber propagation, i.e.,  $P_{\text{rx}}(t) = \varphi P_{\text{tx}}(t)$ , where  $10 \log_{10}(1/\varphi) = \alpha L$  where  $\alpha = 0.35$  dB/km is the attenuation coefficient at 1310 nm.<sup>2</sup>

### III. CHANNEL MODEL

At the receiver, a single photodiode (PD) is used to generate a current  $I(t) = \Re P_{\text{rx}}(t) = \Re \varphi P_{\text{tx}}(t)$ , where  $\Re$  is the responsivity in A/W. The current is then amplified and converted to a voltage  $V(t)$  with a transimpedance amplifier (TIA), with gain  $G$  in units of  $\Omega$ . The gain is set to  $G = (\varphi \Re)^{-1}$  to compensate for losses and PD responsivity. Also, during this process, thermal noise is generated which is modeled by  $N_{\text{th}}(t)$ , a zero-mean white Gaussian random process. Hence, we have  $\mathbb{E}[N_{\text{th}}(t)] = 0$ ,  $R_{\text{th}}(\tau) = \frac{1}{2} N_0^{\text{th}} \delta(\tau)$ , and  $S_{\text{th}}(f) = \frac{1}{2} N_0^{\text{th}}$ . The output of the TIA is then given by

$$V(t) = G (\Re P_{\text{rx}}(t) + N_{\text{th}}(t)) \quad (7)$$

$$= S(t) + S(t) N_{\text{rin}}(t) + G N_{\text{th}}(t), \quad (8)$$

where we use (6) to get from (7) to (8). The voltage  $V(t)$  is then passed through the receiver filter  $h(t)$ . This filter is the matched filter to  $p(t)$ . After filtering, samples are taken at the symbol rate, generating the observations  $Y_k$  (see Fig. 1).

**Theorem 1 (Channel Model).** *The discrete-time equivalent channel model for the system in Fig. 1 is given by*

$$Y_k = A_k + Z_k + Q_k, \quad (9)$$

<sup>2</sup>Another application where high-speed IM-DD transceivers are used is free-space optical (FSO) communications. Our system model can be adapted for FSO links by adjusting  $\alpha$  considering atmospheric attenuation and turbulence.

where  $Q_k$  are independent and identically distributed Gaussian samples  $Q_k \sim \mathcal{N}(0, \frac{1}{2} N_0^{\text{th}} G^2 \|h\|_2^2)$  and  $Z_k$  is a signal-dependent noise term given by

$$Z_k = \sum_{m \in \mathbb{Z}} A_m \int_{-\infty}^{\infty} p((k-m)T - \tau) N_{\text{rin}}(kT - \tau) h(\tau) d\tau. \quad (10)$$

*Proof.* The output of the receiver filter  $Y(t) = (V * h)(t)$  is

$$Y(t) = (S * h)(t) + \underbrace{((S \cdot N_{\text{rin}}) * h)(t)}_{=: Z(t)} + \underbrace{G(N_{\text{th}} * h)(t)}_{=: Q(t)}, \quad (11)$$

where  $Z(t)$  denotes the filtered signal-dependent noise component and  $Q(t)$  the filtered thermal noise. Since  $p(t)$  and  $h(t)$  form a pair of filters that satisfy the zero ISI Nyquist criterion, after sampling at  $t = kT$  ( $k \in \mathbb{Z}$ ), the symbols  $A_k$  are recovered from  $(S * h)(kT)$  in (11). Defining  $Z_k = Z(kT)$  and  $Q_k = Q(kT)$  as the sampled versions of  $Z(t)$  and  $Q(t)$  in (11), respectively, we obtain (9).  $\square$

From (10), we observe that  $Z_k$  depends on neighboring symbols  $A_m$  and their corresponding time-shifted pulses  $p((k-m)T - \tau)$ . Thus, we see via (10) that (9) is not a memoryless channel model, as is usually assumed in the literature, see, e.g., [7]–[9]. While it is straightforward to see that  $Q_k \sim \mathcal{N}(0, \frac{1}{2} N_0^{\text{th}} G^2 \|h\|_2^2)$ , the distribution of  $Z_k$  is not trivial to determine due to its dependence on the transmitted signal  $S(t)$ . The statistical properties of  $Z_k$  are analyzed next.

#### IV. SIGNAL-DEPENDENT NOISE ANALYSIS

RIN noise is often modeled as  $Z_k \sim \mathcal{N}(0, \sigma_Z^2(a_n))$ , where

$$\sigma_Z^2(a_n) = \frac{N_0^{\text{rin}}}{2} a_n^2 \|h\|_2^2. \quad (12)$$

When  $h(t)$  is an ideal brick-wall filter with bandwidth  $\Delta f$  and unit gain,  $\|h\|_2^2 = 2\Delta f$  and (12) results in  $\sigma_Z^2(a_n) = N_0^{\text{rin}} a_n^2 \Delta f$ , which is the expression most often used (e.g., in [7, Eq. (10)], [8, Eq. (8)], and [9, Eq. (8)]), i.e., when  $\sigma_Z^2(a_n)$  depends only on the square of the transmit symbol. If both  $p(t)$  and  $h(t)$  are rectangular pulses in time domain, we see from (10) that  $Z_k$  depends only on  $A_k$ , i.e., the channel is memoryless, and the variance (12) is correct. However, this implies that  $p(t)$  and  $h(t)$  have infinite bandwidth. The rest of the paper is therefore focused on practical band-limited pulses.

Although the channel in (9) generally has memory, we consider here the case where we treat any neighboring symbol interference in the signal-dependent noise component  $Z_k$  as additive noise. This assumption will also be used for the analysis in Sec. V and is explored in the following example.

**Example 1 (Signal-dependent Noise Simulations).** We consider the noise component  $Z_k$  by performing a continuous-time simulation of the model in Fig. 1 with the equally-spaced constellation  $\mathcal{A} = 10^{-3}\{0.55, 0.88, 1.22, 1.55\}$ , along with the parameters specified in Table I. Figure 2 shows the histogram of the received samples  $Y_k$ . The effect of  $Q_k$  is shown by turning off  $Z_k$ , and vice versa. From the histograms, it is clear that the variance of  $Z_k$  depends on the amplitude

TABLE I  
SIMULATION PARAMETERS AND VALUES.

Parameter	Value	Parameter	Value
Modulation order $M$	4	ER	4.5 dB
Symbol rate $R_s$	225 GBd	Noise $N_0^{\text{rin}}$	-140 dB/Hz
Filters $p(t)$ and $h(t)$	RRC	Fiber length $L$	1 km
RRC roll-off	0.1	Attenuation $\alpha$	0.35 dB/km
Samples per symbol	4	Responsivity $\mathfrak{R}$	0.5 A/W
OMA	0 dBm	Noise $(N_0^{\text{th}})^{1/2}$	22 pA/ $\sqrt{\text{Hz}}$

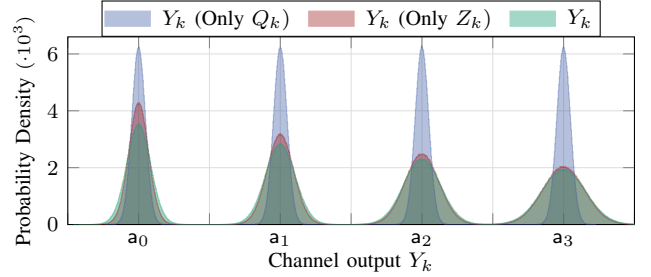


Fig. 2. Histogram of the samples  $Y_k$ . The contributions of the thermal noise  $Q_k$  and signal-dependent noise  $Z_k$  are also plotted independently.

of the transmitted symbol  $A_k = a_n$ : the larger the value of  $a_n$ , the larger the variance.

Motivated by the results in Example 1, we are now interested in the conditional first and second moments of the noise samples  $Z_k$ , conditioned on a given transmitted symbol  $A_k = a_n$ . Using (10), it is straightforward to see that the conditional mean  $\mathbb{E}[Z_k | A_k = a_n] = 0$  because  $N_{\text{rin}}(t)$  is zero-mean. The conditional variance  $\mathbb{E}[Z_k^2 | A_k = a_n]$ , on the other hand, is given by the following theorem.

**Theorem 2 (Conditional Variance of  $Z_k$ ).** The variance of  $Z_k$  conditioned on the symbol  $A_k = a_n$  is given by

$$\sigma_{Z|A}^2(\ell, a_n) = \frac{N_0^{\text{rin}}}{2} \sum_{i \in \mathcal{L}} \sum_{j \in \mathcal{L}} \mathbb{E}[A_i A_j | A_k = a_n] \Psi_{i,j}, \quad (13)$$

when  $\ell \rightarrow \infty$  where  $\mathcal{L} = \{k, k \pm 1, \dots, k \pm \ell\}$  and  $\sigma_{Z|A}^2(\ell, a_n) = \mathbb{E}[Z_k^2 | A_k = a_n]$ . In (13),  $\Psi_{i,j}$  is defined as

$$\Psi_{i,j} = \int_{-\infty}^{\infty} p((k-i)T - \tau) p((k-j)T - \tau) h^2(\tau) d\tau, \quad (14)$$

and the conditional cross expectation in (13) is given by

$$\mathbb{E}[A_i A_j | A_k = a_n] = \begin{cases} m_1^2 & (i \neq j) \wedge (i \neq k \wedge j \neq k), \\ m_1 a_n & (i \neq j) \wedge (i = k \vee j = k), \\ m_2 & i = j \neq k, \\ a_n^2 & i = j = k, \end{cases} \quad (15)$$

where  $m_1 = \mathbb{E}[A] > 0$  and  $m_2 = \mathbb{E}[A^2]$ .

*Proof.* Given that  $R_{\text{rin}}(\tau) = \frac{1}{2} N_0^{\text{rin}} \delta(\tau)$ , the double integral from the expected value of (10) squared, collapses into  $\Psi_{i,j}$ . For the first two cases in (15), i.e.,  $i \neq j$ ,  $\mathbb{E}[A_i A_j | A_k] = \mathbb{E}[A_i | A_k] \mathbb{E}[A_j | A_k]$ . For the last two cases in (15), i.e.,  $i = j$ ,  $\mathbb{E}[A_i A_j | A_k] = \mathbb{E}[A_i^2 | A_k]$ .  $\square$

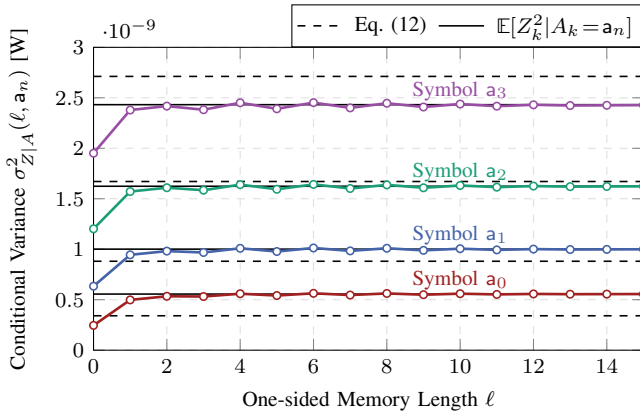


Fig. 3. Conditional variance  $E[Z_k^2 | A_k = a_n]$  using (13) as function of  $\ell$ .

Note that  $\Psi_{i,j}$  (14) is a deterministic quantity, depending only on  $p(t)$  and  $h(t)$ . From (15), it can be seen that the variance (13) will have a polynomial form  $E[Z_k^2 | A_k = a_n] = \frac{1}{2} N_0^{\text{rin}} (p_0 + p_1 a_n + p_2 a_n^2)$ , where  $p_i$  are coefficients that depend on  $m_1$  and  $m_2$ . Hence, we see from (13) that the variance will depend not only on  $a_n^2$  as in the traditional model in (12), but also on a constant  $p_0$  and a scaled version of  $a_n$ .

**Example 2 (Conditional Variance Convergence).** Figure 3 shows (13) as a function of the one-sided memory length  $\ell$  for the same parameters in Table I. The true variance  $E[Z_k^2 | A_k = a_n]$ , with  $\ell \rightarrow \infty$  in (13) (black solid curves), is calculated directly from (9) using a genie-aided approach. The colored curves in Fig. 3 show that (13) converges to the true value when considering  $\ell \geq 12$ . Furthermore, using (12) (black dashed lines) results in an incorrect variance estimate.

## V. INFORMATION-THEORETIC ANALYSIS

The channel in (9) is a channel with memory, and thus, the AIR of interest is the mutual information rate of the input and output defined as [11, Eq. (2)]

$$\mathcal{I}(A; Y) \triangleq \lim_{n \rightarrow \infty} \frac{1}{n} I(\mathbf{A}; \mathbf{Y}), \quad (16)$$

where  $\mathbf{A} = (A_1, A_2, \dots, A_n)$  and  $\mathbf{Y} = (Y_1, Y_2, \dots, Y_n)$ . The channel capacity is the supremum of  $\mathcal{I}(A; Y)$  over all possible input distributions  $P(\mathbf{a})$ , potentially with memory. The optimal decoding rule is given by

$$\hat{\mathbf{a}} = \underset{\mathbf{a} \in \mathcal{A}^n}{\text{argmax}} P(\mathbf{a}, \mathbf{y}) = \underset{\mathbf{a} \in \mathcal{A}^n}{\text{argmax}} P(\mathbf{y} | \mathbf{a}), \quad (17)$$

where we used the fact that  $P(\mathbf{a})$  is constant. The optimal decoding metric is therefore proportional to  $P(\mathbf{y} | \mathbf{a})$ .

### A. Lower Bound via Generalized Mutual Information

A lower bound on  $\mathcal{I}(A; Y)$  can be obtained by using a mismatched decoding metric  $q(\mathbf{a}, \mathbf{y})$  defined as

$$q(\mathbf{a}, \mathbf{y}) = \prod_{k=1}^n q(a_k, y_k), \quad (18)$$

where  $q(a, y) = 1/M \cdot q(y|a)$ . Decoding using the product metric in (18) is suboptimal since it is not proportional to  $P(\mathbf{y} | \mathbf{a})$ . This approach leads to the generalized mutual information (GMI)  $\mathcal{I}_q^{\text{GMI}}$ , which lower bounds the mutual information rate in (16) as [12]–[14]

$$\mathcal{I}(A; Y) \geq \mathcal{I}_q^{\text{GMI}}(A; Y) \triangleq \max_{s > 0} \mathcal{I}_{q,s}^{\text{GMI}}(A; Y), \quad (19)$$

where [15, Eq. (4.35)], [16, Eq. (17)]

$$\begin{aligned} \mathcal{I}_{q,s}^{\text{GMI}}(A; Y) &= E \left[ \log_2 \frac{[q(A, Y)]^s}{\sum_{a' \in \mathcal{A}} P(a') [q(a', Y)]^s} \right] \\ &= \frac{1}{M} \sum_{i=0}^{M-1} \int_{-\infty}^{\infty} p(y|a_i) \log_2 \frac{M [q(y|a_i)]^s}{\sum_{j=1}^M [q(y|a_j)]^s} dy \\ &= \log_2 M + \sum_{i=0}^{M-1} \beta_i, \end{aligned} \quad (20)$$

and where

$$\beta_i \triangleq \frac{1}{M} \int_{-\infty}^{\infty} p(y|a_i) \log_2 \frac{[q(y|a_i)]^s}{\sum_{j=0}^{M-1} [q(y|a_j)]^s} dy. \quad (21)$$

For the channel in Theorem 1, we choose the metric

$$q(y|a) = \frac{1}{\sqrt{2\pi(\sigma_Q^2 + \sigma_Z^2(a))}} \exp\left(-\frac{(y-a)^2}{2(\sigma_Q^2 + \sigma_Z^2(a))}\right), \quad (22)$$

with  $\sigma_Z^2(a) = E[Z_k^2 | A_k = a]$  given by Theorem 2 with  $\ell \rightarrow \infty$ . The metric in (22) therefore adds a second level of mismatch, on top the memoryless mismatch in (18). The metric in (22) makes the assumption that the channel noise can be modeled as Gaussian, which might not be true. Nevertheless, (19)–(22) give a lower bound on the channel capacity, which is what we show in the next section.

### B. Numerical Results

Fig. 4 shows GMI  $\mathcal{I}_q^{\text{GMI}}$  for the parameters given in Table I. We evaluated (19)–(22) using Monte-Carlo integration. Equally-spaced constellations  $\mathcal{A}$  for different values of  $M$  are derived using the constraints given in (1). The following observations are made from Fig. 4. Firstly, lower-cardinality constellations provide higher AIRs except for high OMA values, for which GMI saturates. Secondly, GMI saturates at  $m = \log_2(M)$  for  $M \leq 4$  only, while it saturates at smaller values for higher  $M$ . This saturation for denser constellations can be explained by the signal-dependent noise with higher variance  $\sigma_{Z|A}^2$  in (13) (see Fig. 2) that high-power constellation points experience. This figure shows that using  $M$ -PAM with  $M > 8$  provides only negligible gains, which is in agreement with recent experimental observations in the literature [17, Table I]. Finally, Fig. 4 also shows GMI results when the variance  $\sigma_Z^2(a)$  is calculated via (12) (stars). These results show little difference to those based on Thm. 2, which make us conjecture that taking memory into account is key for this channel model.

To analyze the saturation of the GMI for dense constellations, Fig. 5 shows the saturation values at very large OMA

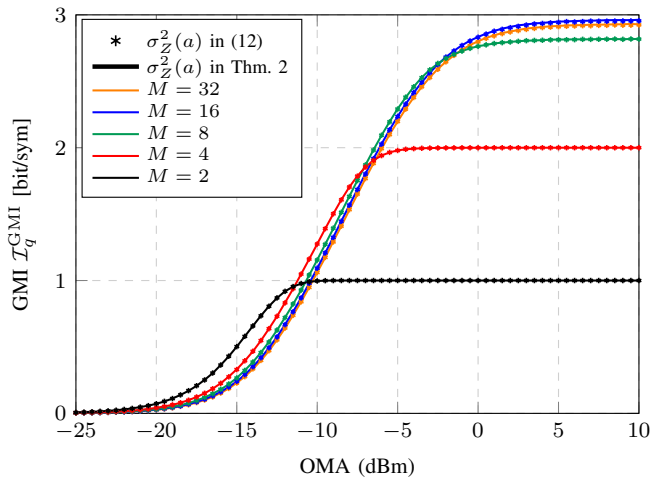


Fig. 4. GMI vs. OMA for the system in Fig. 1 using the parameters in Table I.

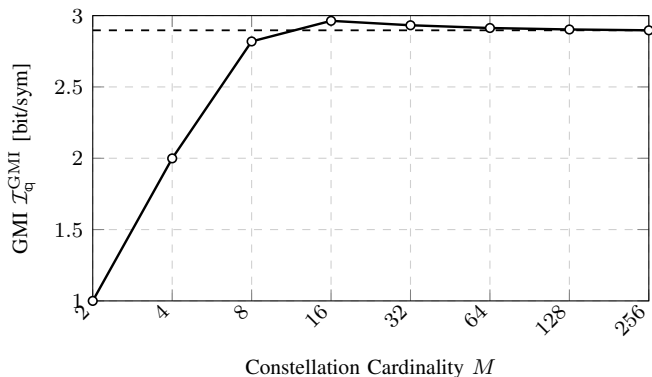


Fig. 5. GMI at OMA = 25 dBm vs.  $M$ . The GMI converges as  $M \rightarrow \infty$  (dashed lines). The maximum value is obtained for  $M = 16$ .

(OMA = 25 dBm). This figure shows that the saturated GMI has a maximum at  $M = 16$ , and confirms that using values of  $M$  larger than  $M = 8$  provides little or no gain in terms of GMI. As mentioned above, we believe that using a mismatched metric with memory would remove this saturation.

To conclude, we study in detail the convergence of the GMI as OMA grows. To this end, we consider 32-PAM with  $s = 1^3$  and analyze the values of  $\beta_i$  in (21). We first show results for the case where the RIN noise is set to zero, i.e., we set  $\sigma_Z^2(a) = 0$ . For this case, Fig. 6 shows results for OMA values of 0, 2, and 4 dBm (gray circles). These results show that as OMA grows, the contribution of the symbols (via  $\beta_i$ ) is symmetric with respect to the middle of the constellation. Furthermore, the outermost constellation points contribute more to the GMI. This is expected, as in this case we are effectively considering an AWGN channel, where the contributions of the inner- and outer-most points at high SNRs (equivalently, high OMAs) only depend on the number of nearest neighbors [18]. Lastly, these results show a clear

<sup>3</sup>The optimum value of  $s$  in the maximization (19) was found to be  $s = 1$  for medium and high OMA values.

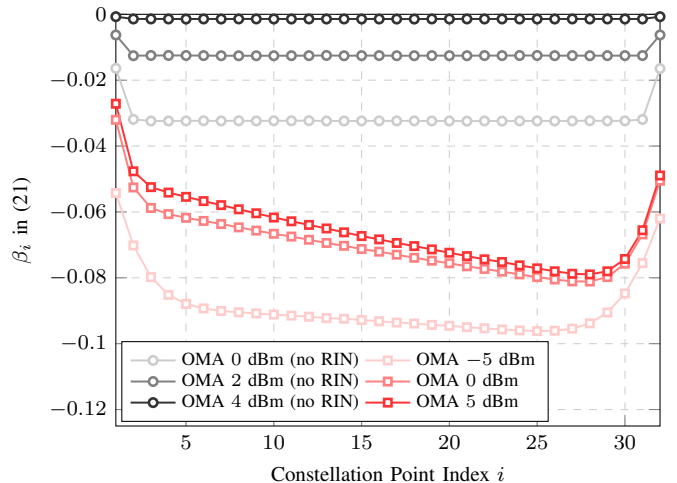


Fig. 6. Contribution of the constellation points via  $\beta_i$  in (21) to the GMI for  $M = 32$ .

convergence of all values of  $\beta_i$  to zero, which results in a GMI saturating at  $\log_2 M$ .

The second set of results in Fig. 6 (red squares) shows the case where RIN is present in the system. The contribution of the constellation points to the GMI in this case changes considerably. First of all, the symmetry with respect to the middle of the constellation is lost, which is caused by the signal-dependent noise. Furthermore, these results show that as OMA grows, the contributions of  $\beta_i$  do not vanish, which explains why the GMI curves in Fig. 6 saturate at values below  $\log_2 M$ . We conjecture that such a detailed convergence analysis could be used, e.g., to design optimal geometrical and/or probabilistic shaping schemes.

## VI. CONCLUSIONS

We provided a novel discrete-time channel model with memory for optical communications with laser relative intensity noise. We derived an analytical expression for the variance of the signal-dependent noise that has a second-order polynomial form in terms of the transmit symbol. This model differs from the standard model in the literature where the variance depends only on the squared symbol. We showed that our model provides a more accurate representation of the continuous-time system. We then studied the GMI for this channel with a memoryless decoding metric. We observed that, for practical system parameters, using PAM modulation with more than 8 points brings negligible gains. Future research avenues include constellation shaping and demapping with memory to improve AIRs of this channel.

## REFERENCES

- [1] X. Zhou, R. Urata, and H. Liu, "Beyond 1 Tb/s intra-data center interconnect technology: IM-DD or coherent?" *J. Lightw. Technol.*, vol. 38, no. 2, pp. 475–484, Jan. 2020.
- [2] D. Che and X. Chen, "Modulation format and digital signal processing for IM-DD optics at post-200G era," *J. Lightw. Technol.*, vol. 42, no. 2, pp. 588–605, Jan. 2024.
- [3] J. Wei, T. Rahman, S. Calabrò, N. Stojanovic, L. Zhang, C. Xie, Z. Ye, and M. Kuschnerov, "Experimental demonstration of advanced modulation formats for data center networks on 200 Gb/s lane rate IMDD links," *Optics Express*, vol. 28, no. 23, pp. 35 240–35 250, Nov. 2020.
- [4] B. Welch, J. Ingham, E. Bernier, and P. Dawe, "Baseline proposals for 200G/L PMD specifications for single wavelength 500 m and 2 km standards," *IEEE P802.3dj Ethernet Task Force*, Feb. 2023.
- [5] G. P. Agrawal and N. K. Dutta, *Semiconductor lasers*. Springer Science & Business Media, 2013.
- [6] Keysight Technologies, *Digital Communication Analyzer (DCA), Measure Relative Intensity Noise (RIN)*, July 2014.
- [7] K. Szczerba, P. Westbergh, J. Karout, J. S. Gustavsson, Å. Haglund, M. Karlsson, P. A. Andrekson, E. Agrell, and A. Larsson, "4-PAM for high-speed short-range optical communications," *J. Opt. Commun. Netw.*, vol. 4, no. 11, pp. 885–894, Oct. 2012.
- [8] G. Rizzelli, P. Torres-Ferrera, F. Forghieri, and R. Gaudino, "An analytical model for performance estimation in modern high-capacity IMDD systems," *J. Lightw. Technol.*, vol. 42, no. 5, pp. 1443–1452, Mar. 2023.
- [9] R. Maneeekut, D. J. Elson, Y. Wakayama, N. Yoshikane, and P. Kaewplung, "Reach extension of a 53.12 Gbps PAM-4 IM/DD signals with optimized extinction ratio in amplified multi-span O-Band transmission," *IEEE Access*, vol. 12, pp. 34 656–34 667, Mar. 2024.
- [10] R. Hui, *Introduction to Fiber-Optic Communications*. Academic Press, 2019.
- [11] H. D. Pfister, J. B. Soriaga, and P. H. Siegel, "On the achievable information rates of finite state ISI channels," in *Proc. IEEE Global Commun. Conf. (GLOBECOM)*, San Antonio, TX, USA, Aug. 2001.
- [12] G. Kaplan and S. Shamai (Shitz), "Information rates and error exponents of compound channels with application to antipodal signaling in a fading environment," *AËU*, vol. 47, no. 4, pp. 228–239, 1993.
- [13] N. Merhav, G. Kaplan, A. Lapidoth, and S. Shamai (Shitz), "On information rates for mismatched decoders," *IEEE Trans. on Inf. Theory*, vol. 40, no. 6, pp. 1953–1967, Nov. 1994.
- [14] A. Martinez, Guillén i Fàbregas, G. Caire, and F. M. J. Willems, "Bit-interleaved coded modulation revisited: A mismatched decoding perspective," *IEEE Trans. Inf. Theory*, vol. 55, no. 6, pp. 2756–2765, June 2009.
- [15] L. Szczecinski and A. Alvarado, *Bit-Interleaved Coded Modulation: Fundamentals, Analysis, and Design*. Chichester, UK: John Wiley & Sons, 2015.
- [16] A. Alvarado, T. Fehenberger, B. Chen, and F. M. J. Willems, "Achievable information rates for fiber optics: Applications and computations," *J. Lightw. Technol.*, vol. 36, no. 2, pp. 424–439, Jan. 2018.
- [17] X. Pang, O. Ozolins, R. Lin, L. Zhang, A. Udalcovs, L. Xue, R. Schatz, U. Westergren, S. Xiao, W. Hu *et al.*, "200 Gbps/lane IM/DD technologies for short reach optical interconnects," *J. Lightw. Technol.*, vol. 38, no. 2, pp. 492–503, Jan. 2020.
- [18] A. Alvarado, F. Brännström, E. Agrell, and T. Koch, "High-SNR asymptotics of mutual information for discrete constellations with applications to BICM," *IEEE Trans. Inf. Theory*, vol. 60, no. 2, pp. 1061–1076, Feb. 2014.